AIAA 2004-####

Computational Hemodynamic Simulation of Human Circulatory System under Altered Gravity

Chang Sung Kim,* Cetin Kiris,† and Dochan Kwak‡
NASA Ames Research Center, Moffett Field, CA 94035-1000

Abstract

A computational hemodynamics approach is presented to simulate the blood flow through the human circulatory system under altered gravity conditions. Numerical techniques relevant to hemodynamics issues are introduced to non-Newtonian modeling for flow characteristics governed by red blood cells, distensible wall motion due to the heart pulse, and capillary bed modeling for outflow boundary conditions. Gravitational body force terms are added to the Navier-Stokes equations to study the effects of gravity on internal flows. Six-type gravity benchmark problems are originally presented to provide the fundamental understanding of gravitational effects on the human circulatory system. For code validation, computed results are compared with steady and unsteady experimental data for non-Newtonian flows in a carotid bifurcation model and a curved circular tube, respectively. This computational approach is then applied to the blood circulation in the human brain as a target problem. A three-dimensional, idealized Circle of Willis configuration is developed with minor arteries truncated based on anatomical data. Demonstrated is not only the mechanism of the collateral circulation but also the effects of gravity on the distensible wall motion and resultant flow patterns.

Introduction

Currently, NASA has been challenging long-duration space missions for the International Space Station (ISS) and flight to Mars. During the elongated space mission, astronauts have to adapt themselves to the altered circumstance of microgravity. Blood circulation as well as body fluids distribution undergoes significant adaptation during and after space flight. Much study on physiological changes under weightlessness has been performed since the early days of the space program [1]. In particular, cardiovascular research in conjunction with the Space Shuttle program has included diverse physiological functions affected by the nervous system such as heart rate, blood pressure, hormone release, and respiration. The altered cardiac output due to adaptation during flight and deconditioning after the flight will impact blood circulation in the human body. Especially, this altered blood supply in the brain and consequent oxygen supply to certain parts of the brain will make non-negligible impact on long-duration flight. Also gravity over 8G causes unconsciousness, so-called, blackout whereas gravity below -3G makes the retina engorged with blood, red-out. To assess the impact of changing gravitational forces on human space and earth flight, it will be essential to quantify the flow characteristics in the brain under varying gravity conditions. Analysis of blood circulation in brain as well as other parts of human body, such as heart, requires the capability to analyze flow in large arteries and capillaries. In addition to the altered gravitational forces, specific shapes and connections of arteries in the brain vary in the human population [2, 3]. Considering the geometric variations, pulsatile unsteadiness, and moving walls, computational approach in analyzing altered blood circulation will thus offer an economical alternative to experiments.

Major technical challenges of the present study relevant to hemodynamics issues can be summarized as i) non-Newtonian modeling of the human blood, ii) distensible wall motion due to heart pulse, iii) capillary bed modeling for outflow boundary conditions, iv) anatomically complex geometry of vascular networks, and v) gravitational effects. Regarding the non-Newtonian modeling, blood flow characteristics are dominated by the behavior of red blood cells since red blood cells constitute the human blood about 40 to 45 percent in volume. Red blood cells aggregation at low shear rates makes apparent blood viscosity rapidly increased. Conversely, the viscosity decreases slowly at higher shear rates with red blood cell deformability. Three different experiments [4-6] in vitro show this so-called shear-thinning phenomenon in Fig. 1.

* RIACS Research Associate, AIAA Member.
† Research Scientist, AIAA Member.
‡ Chief, Advanced Supercomputing Applications Branch, AIAA Member.

Various non-Newtonian models have been developed by curve fitting to the experimental data [7]. They assume in common that apparent blood viscosity is a function of shear rate alone. In the present study, two different models are assessed through steady and unsteady non-Newtonian flow simulations. More details about both models are found in Computational Approach.

Relative diameter change due to the heart pulse is found to be up to about 10 percent in common carotid arteries of young people [8]. Normal arteries have elastic lamina to transfer the blood most efficiently whereas veins have no elastic lamina but valves to prevent reverse flows. Both arteries and veins in vivo show deformable wall motions according to the supine or erect posture under certain gravity. On Earth, gravity pulls down the blood to the feet. In standing posture, the blood pressure in the feet can be high up to 200 mmHg (millimeters of mercury) whereas it is about 60 mmHg in the brain. In space, blood pressure equalizes and becomes about 100 mmHg throughout the human body. Consequently, the arterial wall distensibility due to gravity causes fluid redistribution throughout the whole body. In the present study, a standard first-order approximation [9, 10] to the complex behavior of the arterial wall is adopted by assuming that blood vessels have circular, thin and elastic walls.

To accomplish the simulation at a computationally manageable level, minor arteries such as arterioles, venules, and capillaries need to be truncated. At the truncated positions where flow information is hardly obtainable in vivo, equivalent outflow boundary conditions are required. In this study, a novel approach utilizing the analogy between arterial networks and electric circuits based on Poiseuille's formula is introduced as an alternative to impose adequate outflow conditions. The alternative approaches using the analogy of electric circuits to arterial networks have been presented to supply the boundary conditions for three-dimensional computations [11, 12].

For anatomically accurate three-dimensional reconstruction of complex arterial configuration, image segmentation techniques have been presented using magnetic resonance angiogram (MRA) [12], magnetic resonance imaging (MRI) [13], and computed tomography (CT) [14]. There have been some remarkable studies about computational simulation of the brain circulation [12,15,16]. They assumed the flow Newtonian in large arteries with solid walls. To the authors' knowledge, the present study is the first one to demonstrate the blood circulation in the human brain under altered gravity conditions, by assuming non-Newtonian flow within distensible arterial walls.

Computational Approach

Governing Equations

The flow through the heart and blood vessels is unsteady, viscous, and incompressible. The blood flow through heart and large vessels has been assumed Newtonian and incompressible because blood is a liquid with a viscosity about 3.5 times that of water and acts as a simple fluid with suspended particles such as red blood cells [12-18]. For instance, the Newtonian flows through artificial heart devices have been simulated using the INS3D code [17, 18]. In the present study, the flows of interest are assumed non-Newtonian to account for the shear thinning behavior of the human blood. Governing equations are the three-dimensional, unsteady, incompressible Navier-Stokes equations coupled with non-Newtonian models, and can be written in tensor notation form as:

$$\frac{\partial u_k}{\partial x_k} = 0 \tag{1}$$

$$\frac{\partial u_i}{\partial t} + \frac{\partial}{\partial x_j}\left(u_j u_i\right) = -\frac{\partial p}{\partial x_i} + \frac{\partial \tau_{ij}}{\partial x_j} + g_i \tag{2}$$

The shear stress tensor, τ_{ij} is defined as:

$$\tau_{ij} = \begin{cases} -2\mu S_{ij} & : Newtonian\ flows \\ -2\eta(\dot{\gamma}) S_{ij} & : Non-Newtonian\ flows \end{cases} \tag{3}$$

where μ and η are molecular and apparent viscosity, respectively. S_{ij} is the mean strain-rate tensor and $\dot{\gamma}$ is the shear rate defined as a function of the second invariant of S_{ij} in three-dimensional problems:

$$S_{ij} = \frac{1}{2}\left(\frac{\partial u_i}{\partial x_j} + \frac{\partial u_j}{\partial x_i}\right) \tag{4}$$

$$\dot{\gamma} = 2\sqrt{\mathrm{II}_S} = \sqrt{2\left(S_{ij}S_{ij} - S_{kk}{}^2\right)} \tag{5}$$

Also the body force terms of gravity, g_i are added to Eq.(2) to take gravitational effects into account.

Non-Newtonian models

Two different types of non-Newtonian models are implemented into the INS3D code and assessed through steady and unsteady computations. One is a Carreu-Yasuda model and the other is an extended Casson model. These models have been used in some computational hemodynamic simulations [19-21].

A Carreau-Yasuda model in Eq. (6) describes the shear thinning behavior of blood flows with asymptotic apparent viscosities at zero and infinite shear rates:

$$\frac{\eta-\eta_\infty}{\eta_0-\eta_\infty}=\left[1+(\lambda\dot{\gamma})^a\right]^{\frac{n-1}{a}} \tag{6}$$

where λ and a define the width of the transition region from Newtonian to power-law region, and n-1 is power-law slope as shown in Fig. 1. The constitutive parameters for the human blood are given by:

$$\eta_\infty = 0.00348Pa\cdot s,\ \eta_0 = 0.1518Pa\cdot s,\\ \lambda = 40.0s,\ a = 2.0,\ n = 0.356 \tag{7}$$

For the extended Casson model,

$$\eta=\left(\frac{1}{\dot{\gamma}}\left[C_1(Ht)+C_2(Ht)\sqrt{\dot{\gamma}}\right]^2,\eta_{\max}\right) \tag{8}$$

where Ht is the hematocrit, C_1 and C_2 are coefficients determined for Ht = 40 percent as $C_1 = 0.2(dyn/cm^2)^{1/2}$ and $C_2 = 0.18(dyn\cdot s/cm^2)^{1/2}$ based on the experimental data [5]. To avoid extreme values at lower shear rates, the apparent viscosity is confined within $\eta_{\max} = 0.1518Pa\cdot s$.

Deformable wall model

A first-order approximate model for arterial wall distensibility is adopted based on the assumption of a thin-walled and linearly elastic channel. Although not a complete model of the arterial wall, this approach was found to be a standard first-order approximation to the complex behavior of the arterial wall [9, 10]. Tethering to surrounding structures is thought to reduce the arterial longitudinal motion to a minimum [22]. In the present study, blood vessels are assumed to have circular, thin and elastic walls with negligible longitudinal motion. The increments of blood vessel radius are given by:

$$\frac{\Delta R_i}{R}=\frac{1-\nu_P^2}{E}\frac{R}{h}\left(p_w-\bar{p}_w\right)_i = D_w\left(p_w-\bar{p}_w\right)_i \tag{9}$$

where p_w and $\bar{p}_w$ are transmural and reference pressure at wall, and the arterial wall distensibility D_w is defined as:

$$D_w=\frac{1-\nu_P^2}{E}\frac{R}{h} \tag{10}$$

where h is the wall thickness, E and ν_p are the elastic modulus and Poisson's ratio of the arterial wall, respectively. The arterial wall distensibility is given from $9.45 \sim 26.4\times10^{-7}\,cm^2/dyne$ based on the structural wall properties [10, 23]. For deformable walls, non-slip boundary conditions are replaced by moving wall boundary conditions using the Eq. (9) at each physical time step.

Capillary bed modeling

To make the problem computationally manageable, minor arteries such as arterioles, venules and capillaries need to be truncated. Equivalent outflow boundary conditions should be imposed at the truncated positions. There is an analogy between arterial networks and electric circuits as shown in Fig. 2. A truncated artery is assumed to divide into N branches of same size, for instance, N equals two for bifurcation and three for trifurcation. Under this assumption, the outflow boundary conditions, especially for pressure, can be approximately determined by utilizing this analogy and Poiseuille's theorem:

$$Q=\frac{\pi r^4}{8\mu L}\Delta p \Rightarrow Q=\frac{\Delta p}{\mathbf{R}},\quad Q_{k+1}=\frac{1}{N}Q_k \tag{11}$$

where Q is mass flow rate, p is pressure, and $\mathbf{R}$ is flow resistance. Also r and L are arterial radius and length, respectively. At the k^{th} bifurcation (or trifurcation), its mass flow rate is N times of flow rate through the $(k\text{-}1)^{th}$ branches. Assuming that the flow resistance ratio f is constant, the pressure drop at each level can be expressed in a geometrical series form:

$$\Delta p_{k+1}=\mathbf{R}_{k+1}Q_{k+1},\ \Delta p_k=\mathbf{R}_kQ_k$$

$$\Delta p_{k+1}=\frac{1}{N}\left(\frac{\mathbf{R}_{k+1}}{\mathbf{R}_k}\right)\Delta p_k = f\,\Delta p_k,\ f=\frac{1}{N}\left(\frac{r_k}{r_{k+1}}\right)^4\left(\frac{L_{k+1}}{L_k}\right)$$

$$\Delta p_{Total}=\sum_{k=1}^{\infty}\Delta p_k=\frac{1}{1-f}\Delta p_1=\frac{8\mu L_1}{\pi r_1^4}\frac{Q_1}{1-f}=\frac{32\mu L_1}{1-f}u_1$$

$$\therefore\ \Delta p=\frac{32\mu L}{1-f}u_e \tag{12}$$

To avoid an unrealistic pressure difference between a truncated position and the capillary bed, the flow resistance ratio f should be determined less than one. For the problems with multiple outflow boundaries, it is preferably given by 0.5 ~ 0.95.

MPI-OpenMP parallel processing

An MPI-OpenMP hybrid version of INS3D code [24] was extended with implementation of those numerical approaches, and validated through the comparison with experimental data for both steady and unsteady non-Newtonian cases. Computational experiments have been conducted on the INA Cluster (SGI workstation cluster) at NASA Ames Research Center.

Results and Discussion

Steady non-Newtonian flow

The steady non-Newtonian flow in a carotid bifurcation illustrated in Fig. 3 was simulated as the first validation problem. Anatomically, common carotid arteries (CCA) in pairs arise from the ascending aortas of the heart and connect to the brain through the neck. CCA are divided into internal (ICA) and external carotid arteries (ECA), respectively. Figure 4 shows a chimera overset grid with 8 blocks. Computations are conducted with the same flow conditions of the experiment [19]. In this experiment, a blood analogy fluid (KSCN-X; KSCN-Xanthan gum solution) was used to mimic the shear thinning properties of blood.

The constitutive parameters of the Carreau-Yasuda model in Eq. (7) are modified based on the experimental data as following:

$$\eta_\infty = 0.0022 Pa \cdot s,\ \eta_0 = 0.022 Pa \cdot s,\quad \lambda = 0.11 s,\ a = 0.644,\ n = 0.392 \tag{13}$$

Likewise, a parameter of the extended Casson model is modified as $C_1 = 0.4(dyn/cm^2)^{1/2}$ for this blood analogy fluid.

The Reynolds number based on the CCA diameter is 270, and flow division ratio of ECA over CCA is 0.45. The inflow through the CCA is assumed fully developed. The Figure 5 (a) and (b) show the comparison of axial velocity profiles in the ICA using two different non-Newtonian models. The results of the INS3D with chimera overset grids are compared with those of IFANS3D [25] with multiblock grids, and also compared to the experimental data. Axial velocity profiles are skewed towards the flow divider and the adverse pressure gradient with the increase of the sectional area results in a secondary flow pattern in the sinus. The flow reaccelerates after passing through the maximum diameter region. Overall both the computed results from two different models show an agreement with the experiment. Thus, the Carreau-Yasuda model was mainly used for the computations of non-Newtonian flows.

Unsteady pulsatile non-Newtonian flow

For an unsteady code validation, the pulsatile non-Newtonian flow in a 90 deg circular tube was simulated with the same flow conditions of the experiment [20]. The same blood analogy fluid with the steady case was used and the Reynolds number based on the tube diameter and diastole velocity is 300. The radii of tube and curvature are 4 and 24 millimeters, respectively. For pulsatile inflow boundary conditions, the experimental waveform was successfully regenerated using twelve harmonics based on the Fourier theorem as shown in Fig. 6. Inflows are assumed fully developed and variant with time using the regenerated waveform. Computed results are compared with the experimental data at three different phases: end diastole, peak systole, and begin diastole. Figure 7 shows the comparison of axial velocity profiles on the plane of symmetry and the plane perpendicular to the symmetry plane. The computed results are coincident with the experimental data at all three phases.

Gravity Benchmark Problems

Six-type Gravity Benchmark Problems (GBP) are originally presented to provide the fundamental understanding of gravitational effects on the human circulatory system. As shown in Fig.8, GBP-0 stands for microgravity whereas GBP-1 represents the human body in supine posture under normal gravity on Earth. Among six problems, let us discuss GBP-2 and 3 cases representing the upper and lower part of the human body in standing posture, respectively. Test model is a U-tube with a diameter of 8 millimeters and a curvature ratio of 4. The fluid is assumed Newtonian with a viscosity of 3.5cPoise and the Reynolds number based on the tube diameter is 169. Figure 9 shows a comparison of axial velocity profiles between solid- and deformable-wall cases at 90 deg station. A first-order approximation model in Eq. (9) is adopted for wall moving boundary conditions, and the wall distensibility factor is given about five times larger than that of normal arteries to bring gravitational effects into relief. Even though not all shown here, the gravitational effect on the internal flow within rigid wall is found to be minor.

Table 1. Comparison of required power for GBP-2 and 3.

	Wall	Δp (Pa)	Q (cm^3/s)	$\Delta p\, Q$ (μW)
GBP-2	Rigid	21.4151	3.5186	75.3512
	Deformable	24.8279	3.5186	87.3595
GBP-3	Rigid	21.0905	3.5186	74.2090
	Deformable	19.1109	3.5186	67.2438

For GBP-2W (GBP-2 with deformable wall), however, tube diameter is contracted by 5.1 %D because of the decreased pressure due to gravity. Conversely for GBP-3W, the diameter is expanded by 5.3 %D because of the increased pressure. As flow resistance is, according to Poiseuille's formula, inversely proportional to the fourth order of tube radius, GBP-2W requires about 16% more power whereas GBP-3W requires about 10% less power as shown in Table 1.

GBP provide a preliminary knowledge that gravity has considerable effects on deformable wall motion and con-

sequent flow patterns in the human circulatory system.

Blood circulation in human brain

There are two arteries in pairs that supply blood to the brain. One pair is common carotid artery and the other is vertebral artery. They are distally connected to the important part of the brain, so-called, the Circle of Wills (CoW). The circle is sitting on the base of the brain and its main function is to distribute the blood evenly throughout whole of the brain. Regardless of race or age, its configuration is different among population. Actually it was found that only about 52 percent of the population have an ideal configuration [15, 16]. Thus, as a fundamental approach, an idealized CoW geometry was designed based on anatomical data with minor arteries truncated, not only to demonstrate the gravitational effects on hemodynamics in the brain, but also to simulate the mechanism of collateral circulation in the brain. Figure 10 shows a chimera overset grid with 10 blocks for this ideally balanced configuration. Total number of grid mesh is about 300,000.

Effects of altered gravity

To demonstrate the effects of altered gravity, the computed result under the normal gravity of 1G was simulated and compared with those under microgravity or zero gravity. Figure 11 shows a non-Newtonian flow simulation through the balanced CoW configuration. Because of symmetry, blood flow through the anterior communicating artery (ACoA) is zero. Also the mass flux through the posterior communicating arteries (PCoA) is very low. For distensible wall motions due to the altered gravity, the wall distensibility factor, D_w in Eqs.(9) and (10), was given by $26.4\times10^{-7}\,cm^2/dyne$. To avoid the unrealistic connectivity at the arterial conjunctions, the distensibility factor was set to be zero at each conjunction by assuming that wall distensibility at the conjunction is negligible compared with that of distal arteries. Distensibility factors at the transition region between the conjunction and arterial branches were interpolated using a smoothing function. The decreased blood pressure due to gravity results in arterial contraction up to about 12 %D as zoomed in Fig. 12, which is quite similar to GBP-2W case among six-type GBP.

Collateral circulation

Even though one of main arteries in the brain is stenosed or missing, the distal smaller arteries can receive blood from the other arteries through the CoW. To simulate this interesting mechanism of "collateral circulation" in the brain, the left ICA is presumed occluded 66.7 percent in flow rate. In other words, only one third of the blood is delivered through this artery to the CoW as indicated in Fig. 13. Unlike the balanced configuration case, the mass flux through the PCoA is most increased to compensate about 20 percent for the deficiency. Likewise, blood flow through ACoA is not zero but considerable. Instead, the mass flux through the proximal part of the left anterior cerebral artery (ACA) is very low in order to distribute blood to the left middle cerebral artery (MCA) and left ACA simultaneously. This figure successfully demonstrates the mechanism of collateral circulation in the brain.

** Further computational results and discussion will be presented in the final draft.*

References

1) http://spaceresearch.nasa.gov/research_projects/microgravity.html, and see also http://research.hq.nasa.gov/code_u/nra/current/NRA-01-OBPR-08/AppendixD.html.
2) Alpers, B. J., Berry, R. G., and Paddison, R. M., "Anatomical Studies of the Circle of Willis in Normal Brain," *Arch. Neurol. Psychiatry*, 1959, Vol. 81, pp. 409-418.
3) Gray, H., "Anatomy of the Human Body," 20th Edition by Lewis W.H., Philadelphia: Lea & Febiger, 1918, New York: Bartleby.com, 2000.
4) Chien, S., "Biophysical Behavior of Red Blood Cells in Suspensions," *The Red Blood Cell*, Vol. II, Edited by Surgenor, D. M., Academic Press, New York, 1975, pp. 1031-1133.
5) Merrill, E. W., "Rheology of Blood," *Physiology Reviews*, Vol. 49, 1969, pp. 863-888.
6) Thurston, G. B., "Rheological Parameters for the Viscosity, Viscoelasticity and Thixotropy of Blood, *Biorheology*, Vol. 16, 1979, pp. 149-162.
7) Zhang, J-B, Kuang, Z-B, "Study on Blood Constitutive Parameters in Different Blood Constitutive Equations," *Journal of Biomechanics*, 2000, Vol. 33, pp. 355-360.
8) Reneman, R. S., van Merode, T., Hick, P. *et al.*, "Age-related Changes in Carotid Artery Wall Properties in Man," *Ultrasound in Medicine and Biology*, Vol. 12, 1986, pp. 465-471.
9) Caro, C. G., Pedley, T.J., Schroter, R. C., and Seed, W. A., "The Mechanics of the Circulation," Oxford University Press, Oxford, 1978.
10) Steinman, D. A., Ethier, C. R., "Effect of Wall Distensibility on Flow in a Two-Dimensional End-to-Side Anastomosis," *ASME Journal of Biomechanical Engineering*, 1994, Vol. 116, pp. 294-301.
11) Formaggia, L., Gerbeau, J. F., Nobile., F., and Quarteroni, A., "Numerical Treatment of Defective Boundary Conditions for the Navier-Stokes Equations," *SIAM J. Numer. Anal.* Vol. 40, No. 1, 2002, pp. 376-401.
12) Cebral, J. R., Lohner, R., and Burgess, J., "Computer

Simulation of Cerebral Artery Clipping: Relevance to Aneurysm Neuro-Surgery Planning," Proc. ECCOMAS, Sep. 11-14, Barcelona-Spain, 2000.

13) Taylor, C. A., Draney, M. T., Ku, J. P., Parker, D., Steele, B. N., Wang, K., and Zarins, C. K., "Predictive Medicine: Computational Techniques in Therapeutic Decision-Making," *Computer Aided Surgery*, Vol. 4, No. 5, 1999, pp. 231-247.

14) Quarteroni, A., Tuveri, M., Veneziani, A., "Computational Vascular Fluid Dynamics: Problems, Models and Methods," *Computing and Visualization in Science*, Vol. 2, No.4, 2000, pp. 163-197.

15) Ferrandez, A. and David, T., "Computational models of blood flow in the Circle of Willis," *Computer Methods in Biomechanics and Biomedical Engineering*, Vol. 4 (1), 2000, pp. 1-26.

16) Ferrandez, A., David, T., and Brown, M. D., "Numerical models of Auto-regulation and Blood Flow in the Cerebral Circulation," *Computer Methods in Biomechanics and Biomedical Engineering*, Vol. 5 (1), 2002, pp. 7-20.

17) Rogers, S. E., Kwak, D., and Kiris, C., "Steady and Unsteady Solutions of the Incompressible Navier-Stokes Equations," *AIAA Journal*, Vol. 29, No. 4, 1991, pp. 603-610.

18) Kiris, C., Kwak, D., Rogers, S., and Chang, I-D., "Computational Approach for Probing the Flow Through Artificial Heart Devices," *ASME Journal of Biomechanical Engineering*, 1997, Vol. 119, pp. 452-460.

19) Gijsen, F. J. H., van de Vosse, F. N., and Janssen, J. D., "The Influence of Non-Newtonian Properties of Blood on the Flow in Large Arteries: Steady Flow in a Carotid Bifurcation Model," *Journal of Biomechanics*, 1999, Vol. 32, pp. 601-608.

20) Gijsen, F. J. H., Allanic, E., van de Vosse, F. N., and Janssen, J. D., "The Influence of Non-Newtonian Properties of Blood on the Flow in Large Arteries: Unsteady Flow in a 90 Degree Curved Tube," *Journal of Biomechanics*, 1999, Vol. 32, pp. 705-713.

21) Lei, M., Kleinstreuer, C., and Archie, J. P., "Hemodynamic Simulations and Computer-Aided Designs of Graft-Artery Junctions," *ASME Journal of Biomechanical Engineering*, 1997, Vol. 119, pp. 343-348.

22) Milnor, W. R., "Hemodynamics," 2nd ed., The Williams & Wilkins Co., 1989.

23) Perktold, K., and Rappitsch, G., "Computer Simulation of Local Flow and Vessel Mechanics in a Compliant Carotid Artery Bifurcation Model," *J. Biomechanics*, Vol. 28, No. 7, 1995, pp. 845-856.

24) Kiris, C., and Kwak, D., "Aspects of Unsteady Incompressible Flow Simulations," *Computers & Fluids*, Vol. 31, 2002, pp. 627-638.

25) Kim, C. S., "Sensitivity Analysis for the Navier-Stokes Equations with Two-Equation Turbulence Models and Its Applications," Ph.D. Dissertation, Seoul National University, Seoul, Korea, 2001.

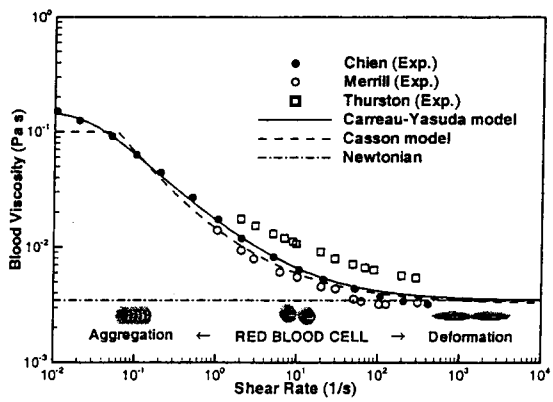

Fig. 1 Logarithmic relation between blood viscosity and shear rate.

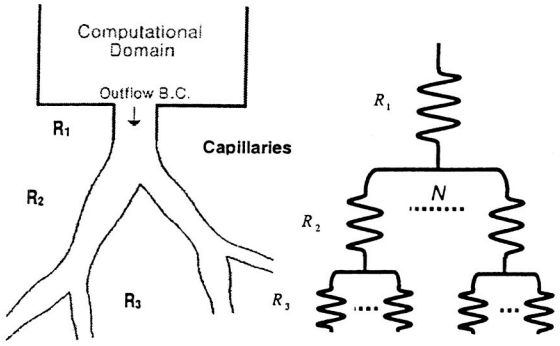

Fig. 2 Analogy of arterial network to electric circuit.

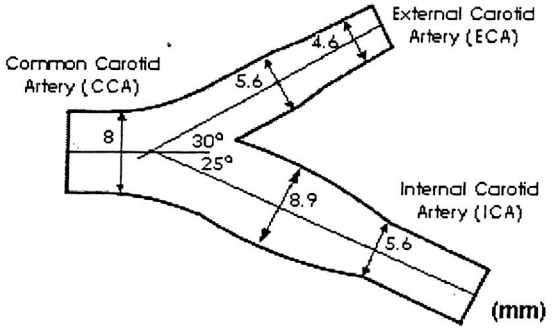

Fig. 3 Schematic definition of a carotid bifurcation.

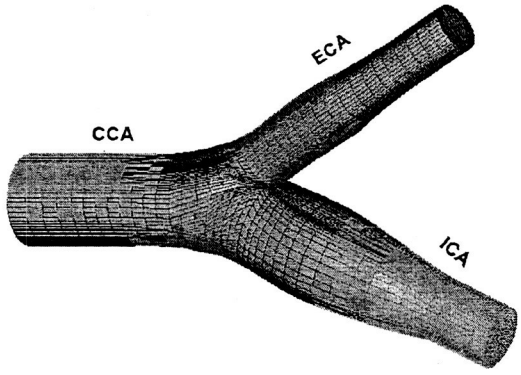

Fig. 4 Chimera overset grid over a carotid bifurcation.

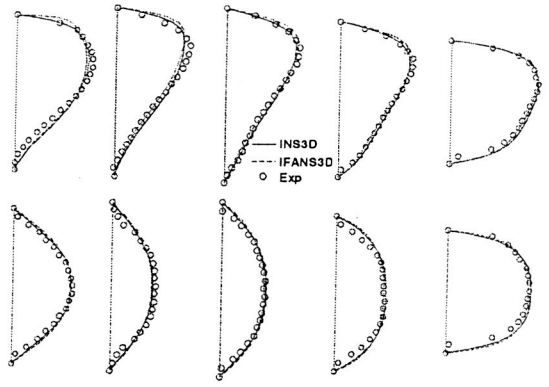

(a) Carreau-Yasuda model

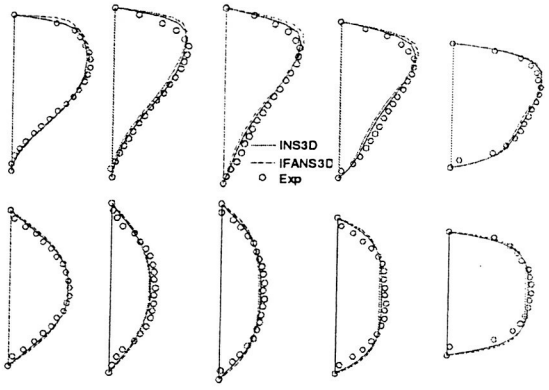

(b) Casson type model

Fig. 5 Axial velocity profiles on the symmetry (upper) and its perpendicular plane (lower) in the ICA.

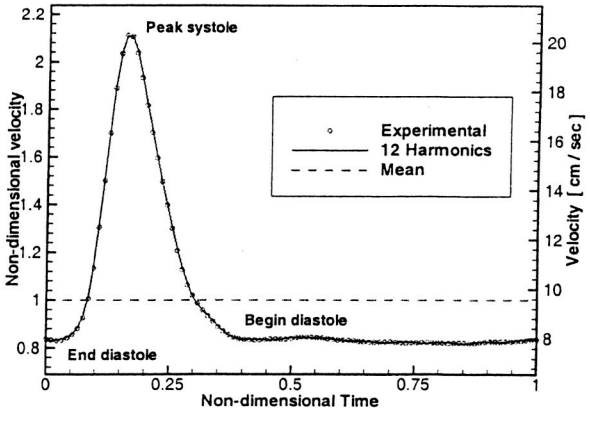

Fig. 6 Inflow waveform regenerated using 12 harmonics.

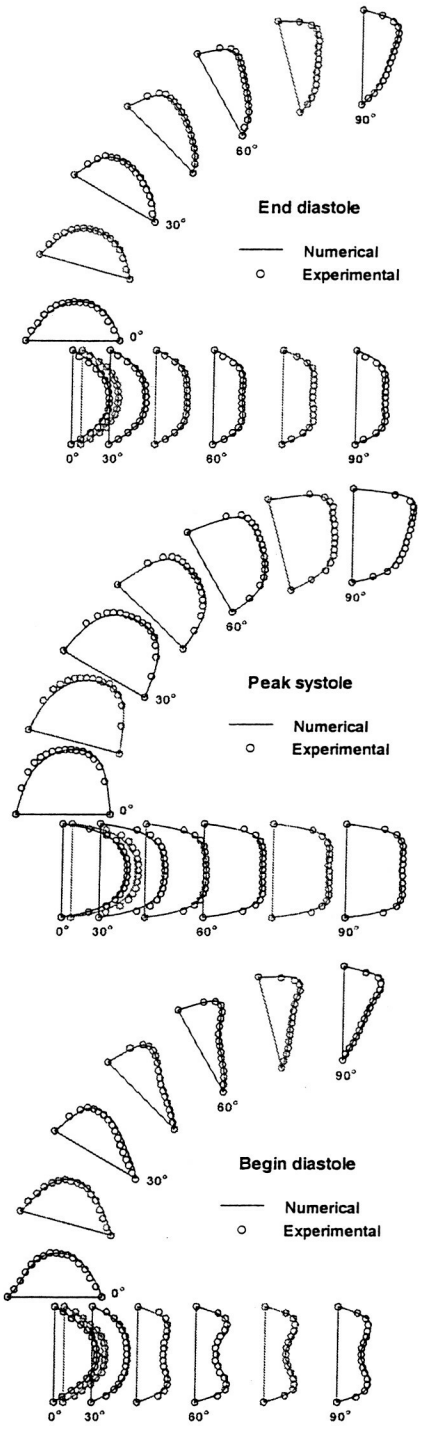

Fig. 7 Comparison of axial velocity profiles between computation and experiment at three different phases.

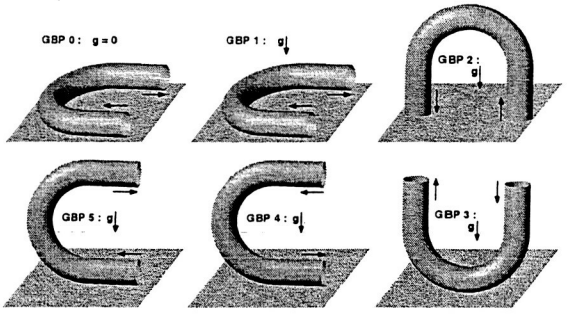

Fig. 8 Six-type gravity benchmark problems (GBP).

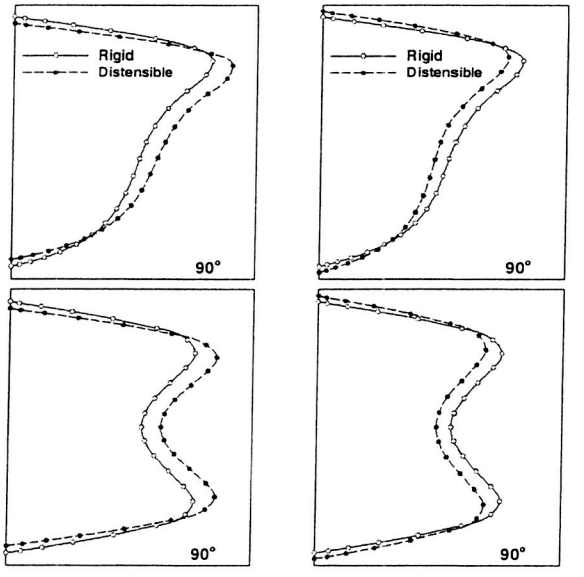

(a) GBP-2 (b) GBP-3

Fig. 9 Comparison of axial velocity profiles between rigid- and distensible-wall cases.

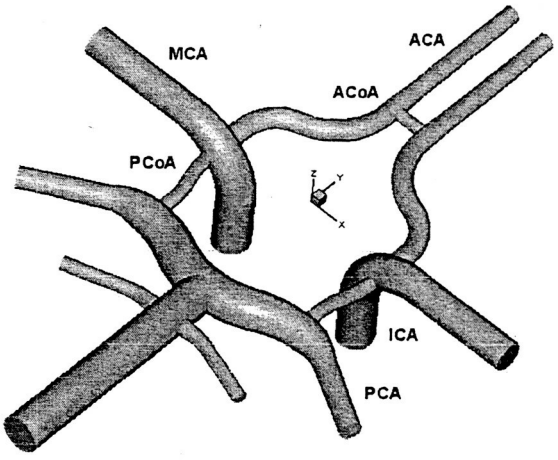

* **ACA**: Anterior Cerebral Artery, **ACoA**: Anterior Communicating Artery, **ICA**: Internal Carotid Artery, **MCA**: Middle Cerebral Artery, **PCA**: Posterior Cerebral Artery, **PCoA**: Posterior Communicating Artery.

Fig. 10 Design of an idealized CoW configuration.

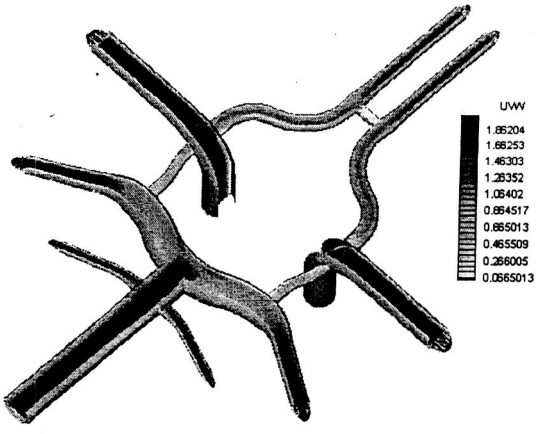

Fig. 11 Non-Newtonian flow simulation through the CoW under 1G.

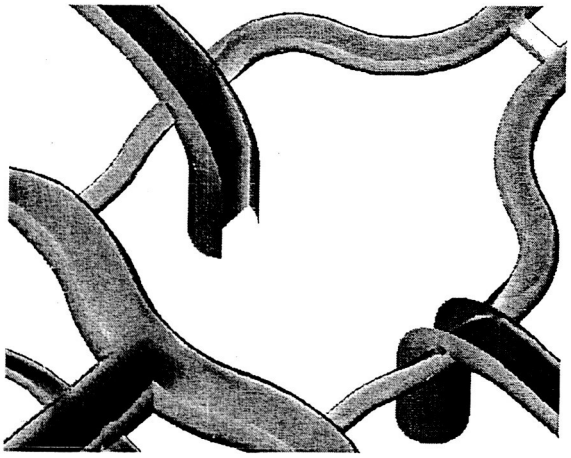

(a) Microgravity (zero G)

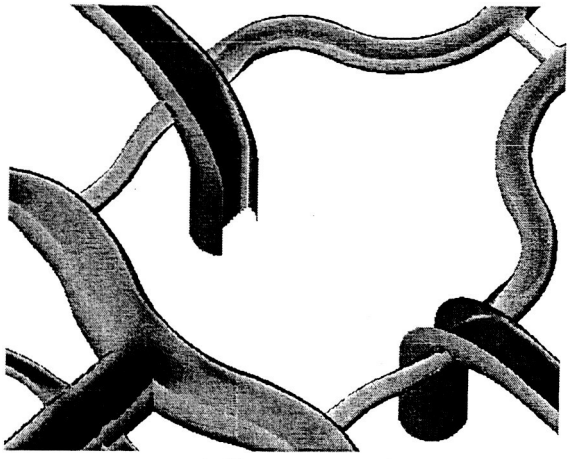

(b) Normal gravity (1G)

Fig. 12 Effects of gravity on arterial wall deformation and flow patterns of CoW. (zoomed view)

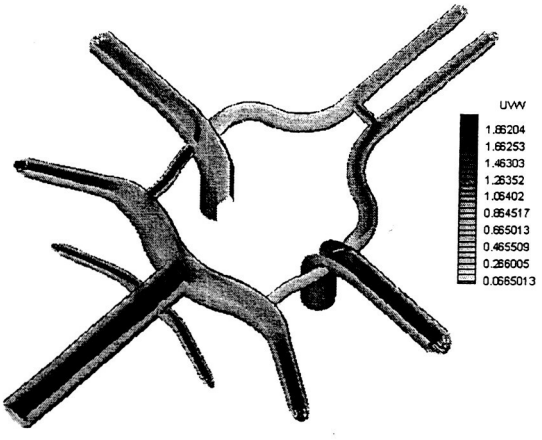

Fig. 13 Collateral circulation through the CoW with left ICA 66.7% stenosed.